CHAPTER 5

SYNTHESIS AND CHARACTERIZATION OF COMPOSITES

$BaTi_{0.85}Sn_{0.15}O_3$ –$NiFe_2O_4$

5.1 INTRODUCTION

Miniaturization of solid-state electronics is achieved by downscaling and multi-functionality. The investigations in the field of multifunctional materials have become very intensive in the last decade. Multiferroics are widely studied in spintronics that need simultaneous ferroelectric and ferri/ferro-magnetic characteristics [137-139]. To advance multiferroicity, one need nano structural multiferroic composite with sizable magnetization and polarization to induce magneto electric (ME) coupling. The ferromagnetic/ferroelectric composite constitutes an ideal interface which dominates both charge and spin dependent multiferroic properties including inter mixing between phases, pinning of ferromagnetic/ferroelectric domains, transmission of strain between component phases, proximity field effects, etc. The multiferroic composites can be formed from several combinations of ferroelectric (such as $BaTiO_3$, $PbTiO_3$ and $BiFeO_3$) and ferromagnetic (such as $CoFe_2O_4$, $NiFe_2O_4$, etc.) [140-142]. Dielectric, electric and magnetic properties of composite systems of nickel ferrite (in doped and undoped form) with ferroelectric/relaxor such as (1-x) $BaTiO_3$/(x)$NiFe_2O_4$[143-150], $BaTiO_3$/$CoFe_{1.8}Zn_{0.2}O_4$ [151], $La_{0.7}Ba_{0.3}MnO_3$/$BaTiO_3$ [152], $MnFe_2O_4$/$(Pb_{1-x}Sr_x)TiO_3$ [153] , $Ba_{0.6}Sr_{0.4}TiO_3$/$Ni_{0.5}Zn_{0.5}Fe_2O_4$ [154], (x) $Mn_{0.5}Zn_{0.5}Fe_2O_4$/ (1-x)$BaTiO_3$ [155], $NiFe_2O_4$/$Pb(Fe_{3/4}Nb_{1/4})O_3$ [156], $CaFe_2O_4$/$BaTiO_3$ [157] , $NiTiO_3$/$NiFe_2O_4$ [158] (x)$Co_{0.8}Ni_{0.2}Fe_2O_4$-(1-x)$Pb_{0.9925}La_{0.005}Zr_{0.55}Ti_{0.45}O_3$ [159], (x)$NiFe_2O_4$-(1- x)$Pb_{0.988}(Zr_{0.52}Ti_{0.48})_{0.976}Nb_{0.024}O_3$ [160], $Ni_{0.9}Co_{0.1}Fe_2O_4$/$Pb(Zr_xTi_{1-x})O_3$ [161], $BiFe_{0.5}Cr_{0.5}O_3$/$NiFe_2O_4$

[162], $Ni_{0.93}Co_{0.02}Mn_{0.05}Fe_{1.95}O_4/Pb(Zr_xTi_{1-x})O_3$ [163], $Pb(Zr_{0.52}Ti_{0.48})O_3/NiFe_2O_4$ [164], $Pb(Zr_{0.52}Ti_{0.48})O_3/NiFe_{1.9}Mn_{0.1}O_4$ [165], $CoFe_2O_4/PbZr_{0.52}Ti_{0.48}O_3$ [166] etc.

Ferroelectric and relaxor materials owing to their various modern technological applications [167,168] have been studied extensively in the last two decades. Barium titanate stannate, $Ba(Ti_{1-x}Sn_x)O_3$ is a binary solid solution system composed of ferroelectric barium titanate and non-ferroelectric barium stannate. Barium stannate titanate is one of the most fascinating and extensively studied relaxor materials, which has already shown its immense potential in many microelectronic devices. It is noticed that increasing of Sn content in BTS ceramic decreased the temperature of ferroelectric-paraelectric phase transition and the maximum of dielectric peaks became more diffuse [169]. Particularly, the relaxor-like behavior can be observed near room temperatures when the Sn concentration is between 10% and 20% . Relaxor ferroelectric exhibit a diffuse peak whose position shift towards to higher temperature with increasing frequency. It has been reported that on the substitution of different concentration of Sn at Ti site of $BaTiO_3$ viz $BaTi_{1-x}Sn_xO_3$ the dielectric constant attains a maximum value of x=0.15 [170].

Nickel ferrite ($NiFe_2O_4$) has an inverse spinel structure in the bulk state [171]. Single crystalline nickel ferrite ($NiFe_2O_4$) which has an inverse spinel structure is reported to show a mixed spinel structure when the grain size is decreased to nanometre range and the magnetic moment at low temperatures is lower than the value of the bulk material [172]. Chinnasamy et al. [173] found a mixed spinel structure for nickel ferrite when the grain size is reduced to a few nanometres. Due to the cation redistribution or change in the coordination of the tetrahedral and octahedral sites, the structure of $NiFe_2O_4$ deviates from an inverse spinel structure to a mixed spinel structure [172]. Among various ferrites, nano size nickel ferrite is a soft magnetic material with low coercive field and saturation magnetization but high electrical resistivity. Hence, it is a suitable

material for magnetic and magneto-optical applications. Nanostructured nickel ferrite exhibits small hysteresis and hence, is considered as a suitable core material for power transformers and telecommunication applications [174]. Nanoparticles of nickel ferrite are also used in gas and humidity sensing, and catalytic applications [175].

To the best of our knowledge dielectric and magnetic properties of composite system of(1-x) $Ba(Ti_{1-x}Sn_x)O_3$+ (x), $NiFe_2O_4$ have there been studied so far. Therefore, in this chapter we have synthesized composites of (1-x) $BaTi_{0.85}Sn_{0.15}O_3$ + (x) $NiFe_2O_4$ (x=5, 10, 15, 20 wt. %). Composition $BaTi_{0.85}Sn_{0.15}O_3$ of $Ba(Ti_{1-x}Sn_x)O_3$ system has been chosen to keep in view that dielectric constant of this particular composition is the highest among the other investigated compositions. Investigation of structural, electrical, dielectric, ferroelectric and magnetic properties of the synthesized composites is discussed in details in the present chapter.

5.2 RESULTS AND DISCUSSION

Constituents of the composites $BaTi_{0.85}Sn_{0.15}O_3$ and $NiFe_2O_4$ have been referred throughout the text and figures by abbreviated name BTS and NF whereas their composites (1-x) $BaTi_{0.85}Sn_{0.15}O_3$ + (x) $NiFe_2O_4$ (x= 5, 10, 15 and 20 %) by BTS-NF5, BTS-NF10, BTS-NF15, and BTS-NF20, respectively.

5.2.1 Thermal Analysis of Mixture of BTS and NF15

Figure 5.1 shows the TGA-DSC curves of one of the composite BTS- NF15. TGA curve shows a weight loss approximately 2.2% below 200°C which corresponds to the evaporation of the remaining acetone and physic-adsorbed water molecules from the atmosphere on the surface of the particles of BTS or NF or both. Another weight loss approximate 1 % in the temperature range 400^oC-800^oC may be due to the expulsion of gasses such as CO_2, NO_2 adsorbed by the powder. Thereafter, the weight of the powder remains constant up to 1000^oC.The absence of any

exothermic or endothermic peak in the DSC curve confirms that in the temperature range 25 to 1000^{o}C no chemical reaction is taking place between constituents of the composite.

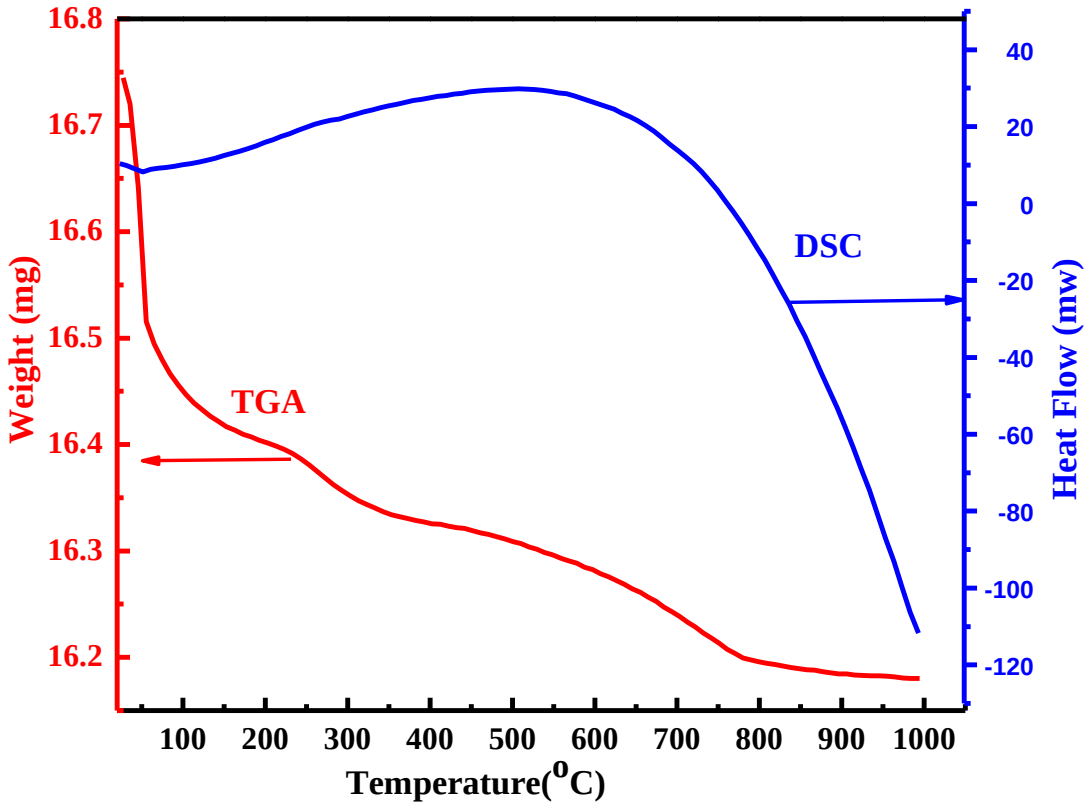

Figure 5.1 TGA-DSC Curve of mixture of BTS+NF15

5.2.2 Phase Analysis and Crystal Structure

The room temperature X-ray diffraction pattern of the relaxor-ferroelectric phase (BTS), ferrite phases (NF) and their composites are shown in Figure 5.2. All the peaks that appear in the XRD patterns have been identified. The peaks present in the XRD pattern of ferrite phase (NF) has been indexed on the basis of JCPDS file no.10-0325 for cubic spinel structure of $NiFe_2O_4$ [171]. XRD pattern of relaxor phase (BTS) was compared with JCPDS file no. (05-0626)

reported in the literature for the cubic phase of perovskite $BaTiO_3$. The XRD patterns of the composites containing peaks of cubic perovskite BTS and spinel NF. Therefore, is clear that there is no intermediate phase or interphase formed in the composites. No structural change is also observed for both the relaxor phase (BTS) as well as ferrite phase (NF) in the composites. In the case of relaxor phase, (110) peak is most intense and in the case of ferrite sample, (311) peak is most intense. As the content of ferrite phase increases in the composite, the intensity of the ferrite peaks (311) increases. Using the height of intensity peak corresponding to (311) reflecting plane of BTS and (110) plane of $NiFe_2O_4$, the approximate amount of ferrite and relaxor phases present in the composites have been calculated using the following relations

$$Phase\ fraction\ of\ NF = \frac{I_{(311)NF}}{I_{(311)NF} + I_{(110)BTS}}\ x\ 100 \qquad (5.1)$$

$$Phase\ fraction\ of\ BTS = \frac{I_{(110)BTS}}{I_{(311)NF} + I_{(110)BTS}}\ x\ 100 \qquad (5.2)$$

The calculated percentages of BTS and NF phases in the composites are presented in Table 5.1. It is evident from Table 5.1 that the percentage of ferrite and relaxor phase in the composites is approximately equal to their weight percentage taken for the synthesis of composites. This again suggests that the particulate composite formation during sintering of the mixture is not leading to any new phase.

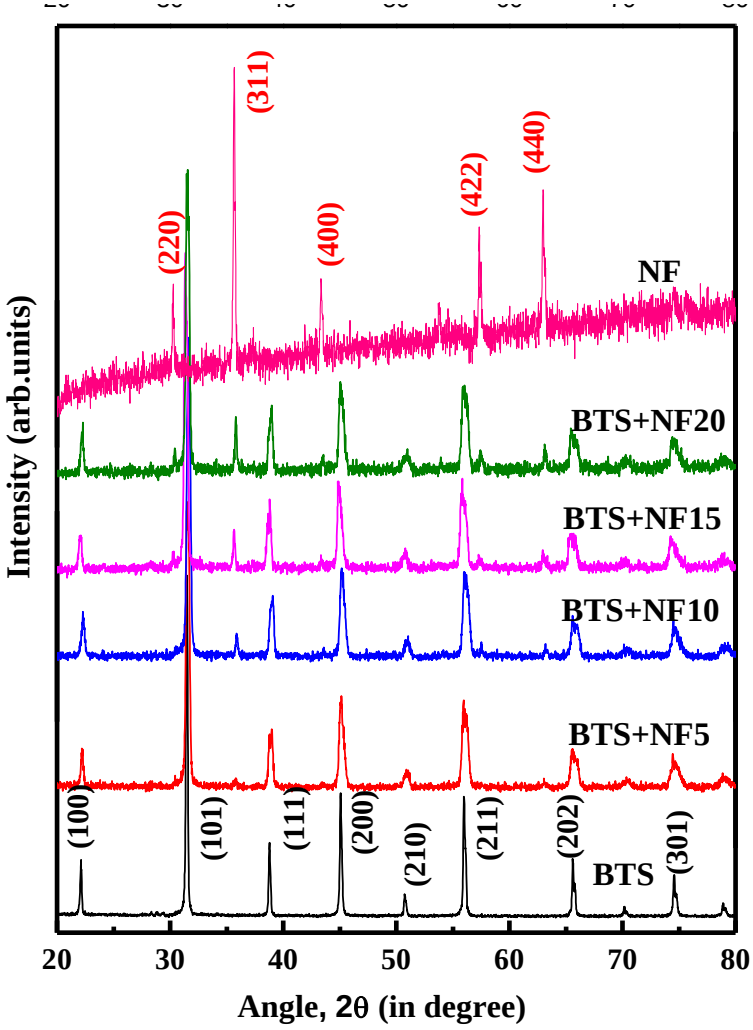

Figure 5.2 The x-ray diffraction pattern of composites and their end members.

Table 5.1 Intensity of XRD peak corresponding to BTS and NF phases present in particulate composites of $BaTi_{0.85}Sn_{0.15}O_3$ and $NiFe_2O_4$

Sample Code	$I_{(110)}$ of BTS Phase	$I_{(311)}$ of NF Phase	% Phase fraction of BTS	% Phase the fraction of NF	Nominal weight % ratio of BTS: NF
BTS+NF5	5573	326	94.4	5.6	95:5
BTS+NF10	6236	670	90.3	9.7	90:10
BTS+NF15	6300	1096	85.2	14.8	85:15
BTS+NF20	5347	1347	79.9	20.1	80:20

The average crystallite size (D) of the sintered samples of BTS, BTS-NF5, BTS-NF10, BTS-NF15, BTS-NF20 and NF was calculated using Equation 2.2. These values are given in Table 5.2.

5.2.3 Density and Porosity Measurement

The theoretical density (d_{th}) of the samples was computed from the Equation (5.3).

$$d_{th} = (1-x)\left[\frac{M_{FE}}{N_a {a_{FE}}^3}\right] + (x)\left[8\frac{M_F}{N_a {a_F}^3}\right] \quad (5.3)$$

Where M_{FE}-molecular weight of relaxor phase (BTS), M_{FE},-molecular weight of ferrite phase (NF), a_{FE} - lattice constant of ferroelectric phase (BTS), a_F – lattice constant of ferrite phase (NF)

N_a – Avogadro's number

The values of theoretical density (d_{th}) are given in Table 5.2. It is observed that the theoretical density increases with increase in ferrite content x in composites. The experimental density (d_b) of the samples BTS, NF and their composites were obtained using Archimedes principle, and the values are summarized in Table 5.2. The experimental density increases with increase in ferrite content x in the composite. The % porosity was calculated using the Equation (2.3). The bulk

density, theoretical density and % porosity of all the samples are presented in Table 5. 2. It can be noted that with an increase in the $NiFe_2O_4$ content, the density of the composites increases and hence % porosity decreases. This may be attributed to higher sinterability of $NiFe_2O_4$ in comparison to $BaTi_{0.85}Sn_{0.15}O_3$.

Table 5.2 Lattice parameter, crystallite sizes and grain size, theoretical density, bulk density and % porosity of constituent phases and their composites.

Sample Code	**Lattice parameter (Å)**		**Grain size (µm)**	**Theoretical density, d_{th} (g/cm^3)**	**Bulk density, d_b (g/cm^3)**	**Porosity %**
	BTS	**NF**				
BTS	4.0218	-----	4	6.21	5.55	11
BTS-NF5	4.0246	8.3058	1	5.94	5.33	10
BTS-NF10	4.0261	8.3291	1	5.66	5.17	9
BTS-NF15	4.0277	8.3394	1	5.37	5.09	5
BTS-NF20	4.0289	8.3431	1	5.19	4.98	4
NF	-------	8.3666	2	5.38	5.05	6

5.2.4 Fourier Transform Infrared (FTIR) Spectroscopy

For recording FTIR spectrum of the powders of sintered samples, small amounts of the powders were mixed with KBr and pelletized using a hydraulic press. FTIR spectrum of the KBr mixed powders was recorded in the wave number range 400 - 4000 cm^{-1}. FTIR spectrum of samples BTS, NF, and their composites are shown in Figure 5.3. The spectrum of samples BTS and NF were compared with the FTIR spectrum of $BaTiO_3$ and $NiFe_2O_4$ reported in the literature [176,177]. It is noted down that in the spectrum of BTS an intense peak around 540 cm^{-1}appears

which is assigned to TiO_6 vibration that connected to the barium ion. The spectrum of NF exhibited an intense band at 607 cm^{-1} which correspond to the Fe-O bond [177]. FTIR spectra of composite samples contain no other additional peak than the absorption bands of constituent phases. Further, it is noted down that the position of bands corresponding to BTS and NF phases remains same in the composites, which supports the negligible interdiffusion between the constituent phases. A weak intensity peak presents in the spectrum of all the samples around 2350 cm^{-1} indicates the presence of CO_2 gas in the chamber of spectrometer [178].

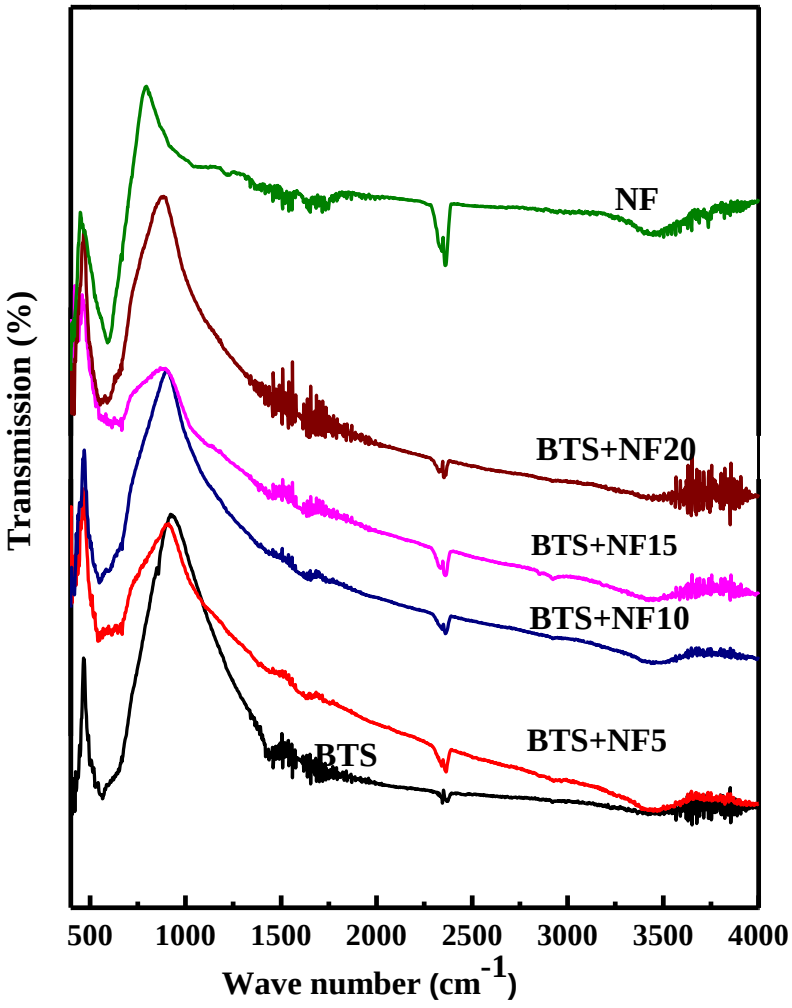

Figure 5.3 FTIR spectrums of composites and their end members.

5.2.5 Morphological Analysis

Scanning electron micrographs (SEM) of the fractured surfaces of BTS, NF, and their four composites are shown in Figure 5.4. Both BTS and NF have well-developed microstructure but grains morphology is different. SEM image illustrates that BTS grains are uniform and spherical in shape. In the scanning electron micrograph (SEM) of NF, octahedron faces and agglomeration of grains are clearly visible. In the SEM of the composites, two separate constituent phases could be clearly noticed, the one with rounded particles that belongs to BTS and the other one with octahedral shape that belongs to ferrite (NF), demonstrating that composites were obtained with a good dispersion of the nickel ferrite spinel phase in the BTS relaxor matrix. No distinct grain boundaries are observed in the SEM of the composite. The microstructure of the composites appears denser in comparison to their constituent phases which are in agreement with the results presented in Table 5.2 (obtained using XRD data). The average grain size of the composites and their constituent phases obtained by linear intercept method is given in Table 5.2.

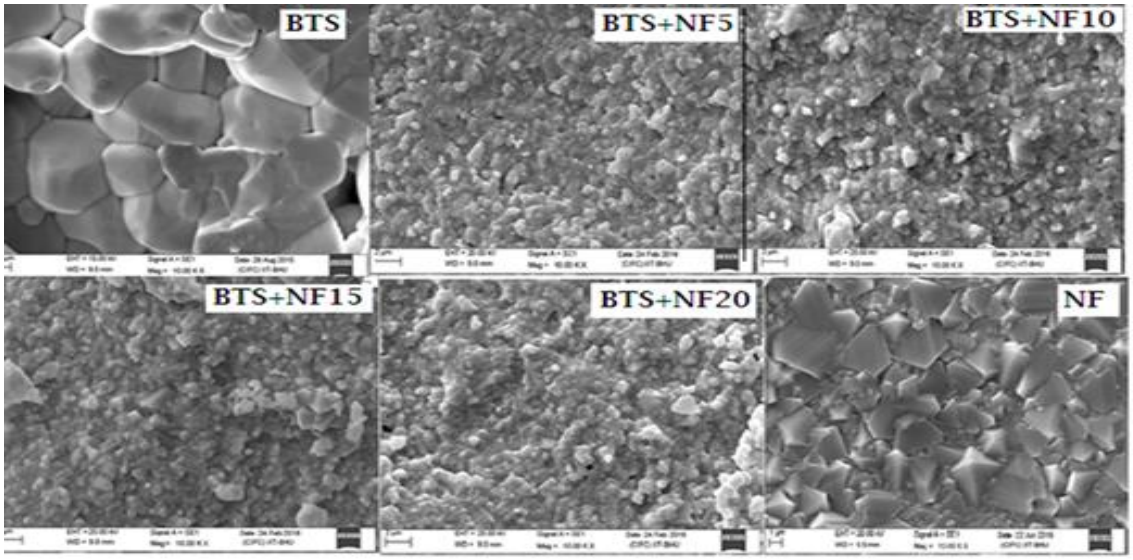

Figure 5.4 Scanning electron micrographs of the fractured surface of pellets of composites and their members

5.2.6 Energy Dispersive X-ray (EDX) Analysis

In order to check the compositional homogeneity of the synthesized powders, the compositional variation in terms of the concentration profile of the elements has been probed using Energy Dispersive X-ray Analysis (EDXA) technique. Typical EDXA spectra of the samples are shown in Figure 5.5. It is noted that only the peaks of elements such as Ba, Ti, Ni, Fe, Sn, and O are present at their respective band energy [176-177]. The quantitative composition of the composite was obtained from EDX data. The observed atomic percentage of the elements is exactly matched to our initial experimental data which confirmed the purity of the constituent phases and their composites.

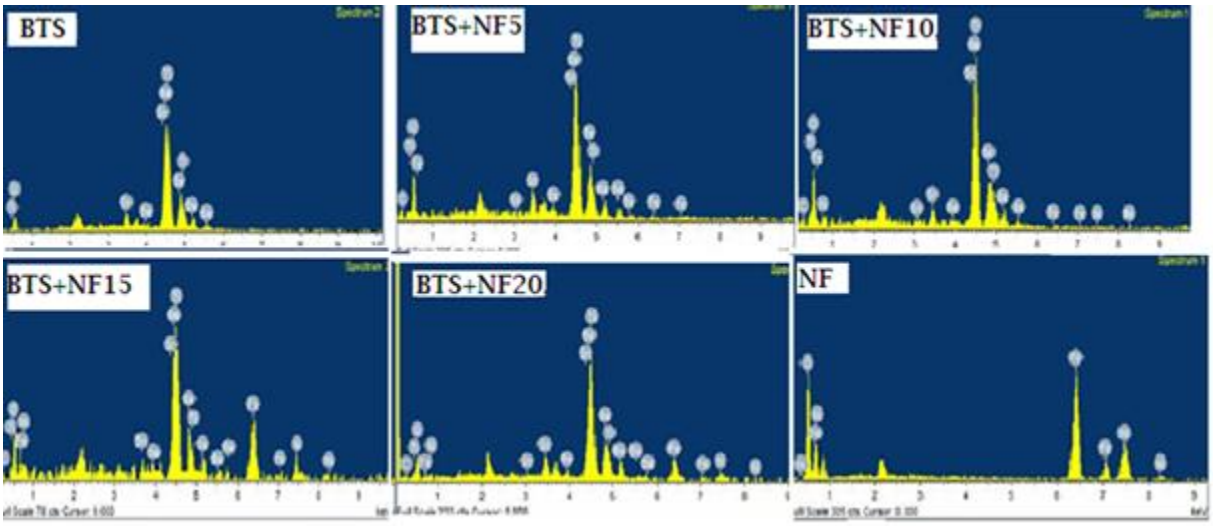

Figure 5.5 Energy dispersive x-ray analysis (EDXA) spectrums of sintered samples

5.2.7 AC Conductivity

AC conductivity (σ_{ac}) analysis of constituent relaxor phase BTS and the composites has been carried out to understand conduction mechanism involved in these samples. The variation of ac conductivity with frequency for BTS and one of the composites BTS + NF15 at different temperatures is shown in Figure 5.6 (a) and (b),

respectively. Similar behavior was observed for other composites also. The total conductivity of a polycrystalline ceramic system has contributions of grain, grain boundary, and electrode-ceramic interface. The contribution of electrode-ceramic interface for the sample BTS is ruled out because the current was found to be independent of time by applying the voltage. Therefore, the conductivity spectrum of the sample BTS should ideally show two dispersion regions. The first plateau in the low-frequency region represents the total or direct bulk conductivity (σ_{dc}) followed by a dispersion region due to the effect of grain conductivity and grain boundary relaxation processes. The second plateau after this dispersion region corresponds to the grain contribution to the bulk conductivity of the samples, and the successive dispersion after the second plateau in the high-frequency region shows the dielectric contribution through the grain relaxation.In the conductivity spectra of BTS sample, at temperatures below 150^{o}C, conductivity almost linearly varies with frequency, above this temperature a low-frequency dispersion followed by a plateau and again a dispersion in the high-frequency range is seen. The second plateau in the high-frequency regime (as mentioned above) could not be observed due to limited frequency range available in the instrument used in this work. The conductivity plot of the composite BTS+NF15 exhibits the following characteristic features. In the low-frequency region dispersion is observed while at higher frequencies, curves appear to merge for all temperatures indicating the presence of multiple relaxation and thermally activated processes in the composite. Similar results of the ac conductivity have been reported for other relaxor-ferrite composite [178-179]. The Linear variation of σ_{ac} with frequency indicates that the conduction occurs by the hopping of electrons between ions of the same element present in more than one valence state, distributed randomly over crystallographically equivalent lattice sites. In relaxor sample $BaTi_{0.85}Sn_{0.15}O_3$ (BTS), elements Sn and Ti are multivalent ions, therefore hopping of electrons

between Sn^{2+} and Sn^{4+} ions; Ti^{3+} and Ti^{4+} ions may take place. Similarly in the composites two more multivalent ions such as Ni^{2+}, Ni^{3+}, Fe^{2+} and Fe^{3+} due presence of ferrite phase. In hopping conduction mechanism, the increase in drift mobility of charge carriers results in an increase of conductivity with increase in temperature.The value of the log σ_{ac} (at room temperature and 20 Hz) of the samples is reported in Table 5.3. It is noticed from the Table 5.3 that conductivity of all the composites is less than the conductivity of relaxor BTS phase. Generally, it is expected that an increase of conductivity with the increasing nickel ferrite content. The observed slightly less value of conductivity of the composites as compared to BTS might be due to the accumulation of a different number of impurities and defects (especially the oxygen vacancies) at the interfaces of the grains which is hard to control during the sintering process

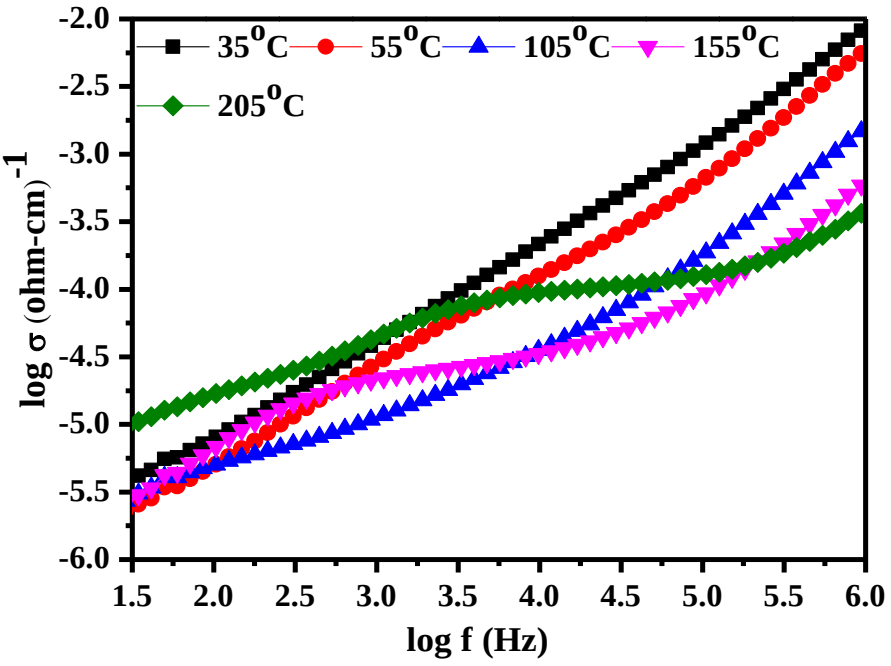

Figure 5.6 (a) For BTS variation of the logarithm of conductivity, σ_{ac} with the logarithm of frequency at different temperatures

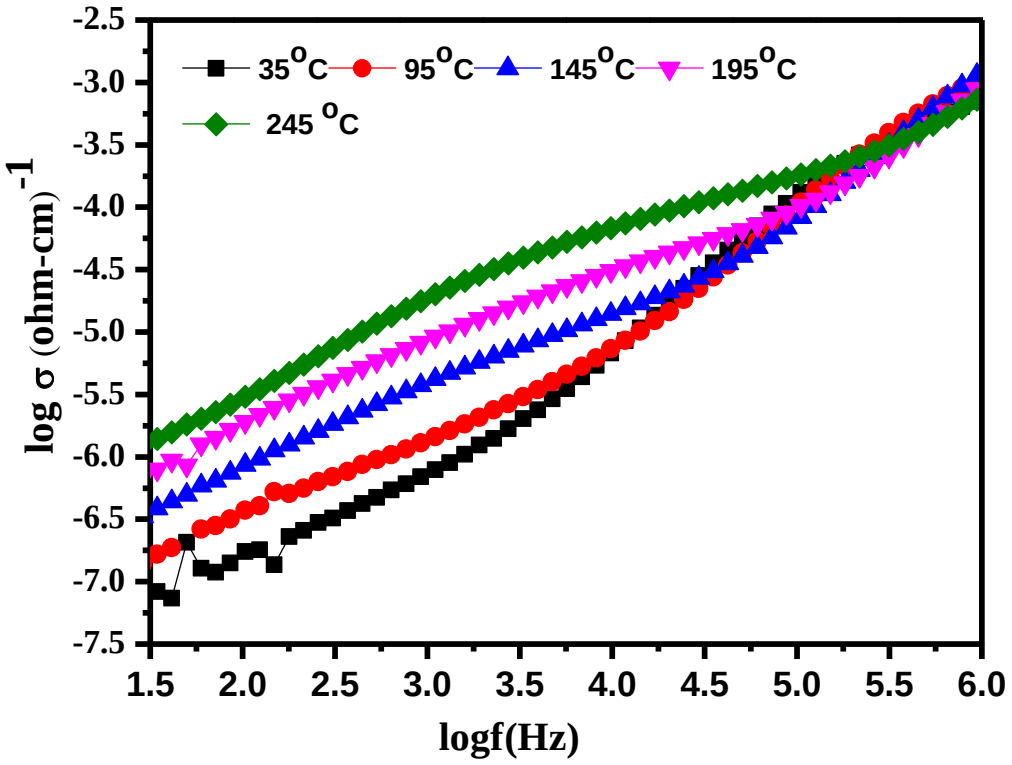

.

Figure 5.6 (b) For BTS+NF 15 variation of logarithm of conductivity, sac with logarithm of frequency at different temperatures

5.2.8 Dielectric and Ferroelectric Properties

The variation of the dielectric constant (ε_r) and dissipation factor (D) for $BaTi_{0.85}Sn_{0.15}O_3$ (BTS) and composites at 1 kHz frequency is shown in Figure 5.7. For the comparison variation of the dielectric constant (ε_r) and dissipation factor (D) for NF at 1 kHz frequency is shown in the inset of Figure 5.7. Figure 5.7 reveals that the dielectric constant of BTS sharply decreases with increasing temperature. It is reported in the literature that Sn doping on Ti site of $BaTiO_3$,

ferroelectric to paraelectric transition temperature shifts towards lower temperature and a transition temperature for $BaTi_{0.85}Sn_{0.15}O_3$ is below the room temperature therefore BTS at and above room temperature is in paraelectric state. Variation of the dielectric constant of composites remains almost constant up to 120^{o}C but starts to increase at a higher temperature. Since the charge hopping is a thermally activated process; dielectric polarization increases with increasing temperature resulting in an increase in dielectric constant. Dielectric constant (at room temperature and 1 kHz) of all the samples is given in Table 5.3, the value of dielectric constant of the composites and NF is lower than the dielectric constant of BTS. The lower value of dielectric constant of the composites is attributed to the lower value of the conductivity of these samples as compared to the value reported in Table 5.3 of BTS. The variation of dissipation factor, D with temperature is similar for BTS, composites, and NF. Dissipation factor remains constant up to 120^{o}C and thereafter starts increasing with increasing temperature. From Table 5.3 one can notice that value of dissipation factor (at RT and 1 kHz) of the composites is lower than that for BTS which is also attributed to the low conductivity of the composites. Almost temperature independent, the high value of dielectric constant (~1000) and low loss of these composites makes them useful for the application of thermally stable capacitor.

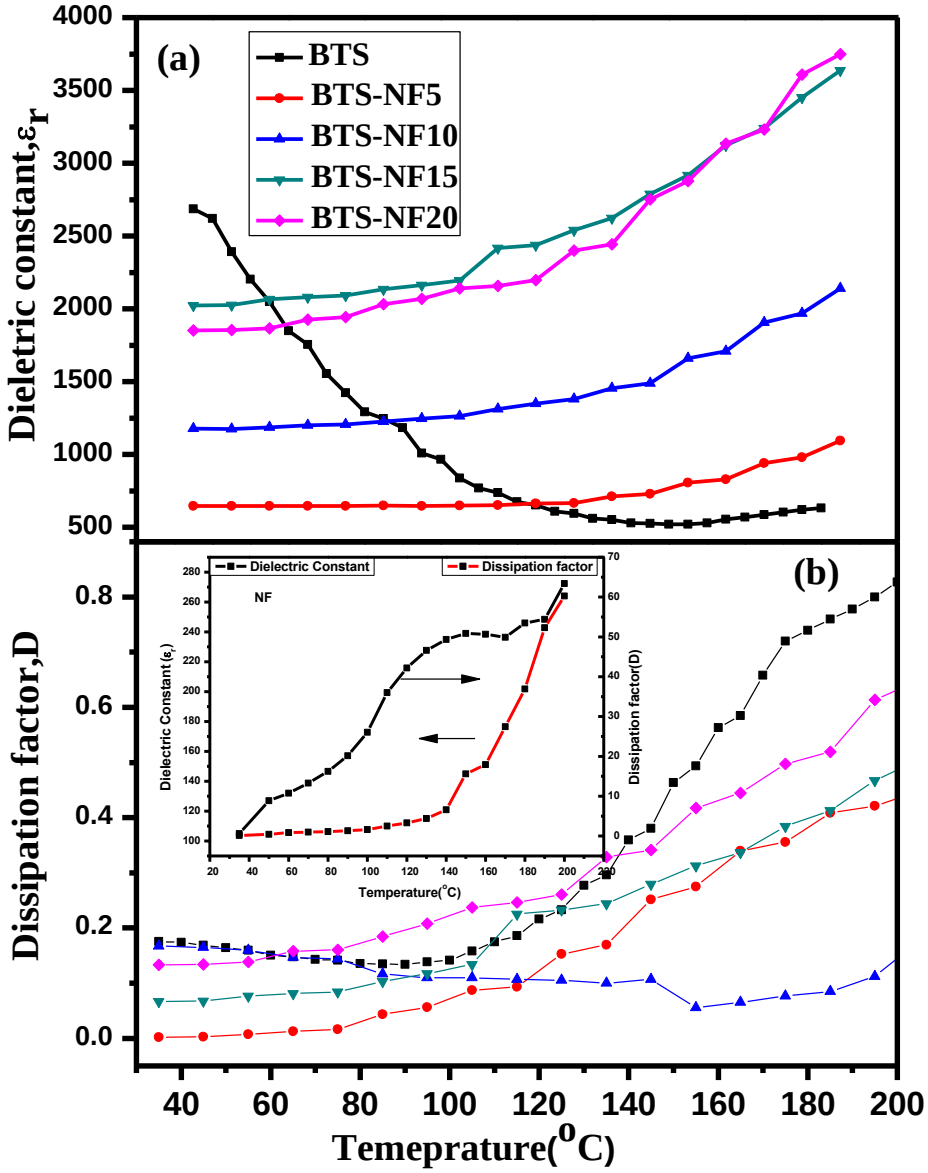

Figure 5.7 Variation of (a) Dielectric constant and (b) Dissipation factor with temperature of samples at 1 kHz

Figure 5.8 and 5.9 shows a variation of dielectric constant and dissipation factor with frequency at few selected temperatures for BTS and one of the composites BTS+NF15, respectively. Similar behavior was observed for other composites also. The dielectric constant of BTS decreases with an increase in the frequency upto 10 kHz and becomes constant above 10 kHz. The dielectric constant of composite BTS+NF15 also decreases with increasing frequency upto 10 kHz and remains constant in the frequency range 10 -100 kHz, thereafter again starts increasing with increasing frequency. The large values of dielectric constant in the low-frequency region of BTS and composites can be associated with the space charge polarization and inhomogeneous dielectric structure. These inhomogeneities arise from impurities, grain structure and pores [179]. The space charge polarization dominates at low frequency and high temperature. The decrease in dielectric constant with frequency can be explained by Koop's theory [180], which considers the dielectric as the Maxwell–Wagner type inhomogeneous medium of two layers [181,182]. According to this model, the dielectric structure contains conducting grains which are separated by insulating grain boundaries. At lower frequencies, the effect of grain boundaries dominates over grains. If the resistance of the grain boundary is high, the electrons reach the grain boundaries through hopping, pile up and hence, in turn, produce polarization which accounts for the high value of dielectric constant [183,184]. However, as the frequency increases, the decrease in dielectric constant is observed because, at high frequencies, the electrons at the grain boundaries generally reverse their direction of motion. This reduces the probability of electrons reaching the grain boundary and hence results in the reduction in the dielectric constant. In composite beside polarization due to different electrical properties of grains and grain–boundaries, space charge polarization effect that the interface of the BTS and

NF will also contribute, hence strong dispersion is observed in the composite as compared to BTS.

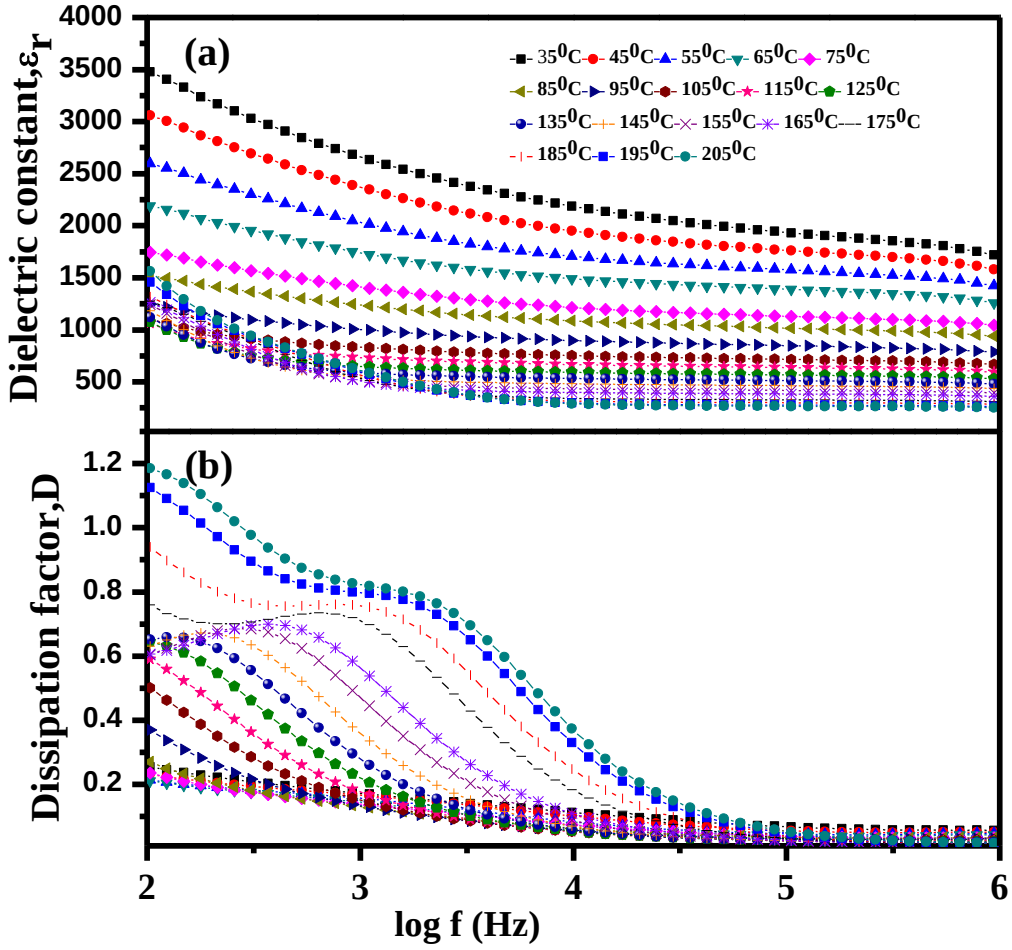

Figure 5.8 For BTS variation of (a) dielectric constant and (b) dissipation factor with logarithm of frequency at different temperatures

In the D vs. log f plot of BTS, a peak is observed at all the temperatures. With increasing temperature, the position of peak shifts to the higher temperature side along with the significant frequency dispersion. This suggests the relaxor nature of the BTS which is in agreement with the literature [110]. Dissipation factor, D vs. log f plot of the composite BTS+NF15 exhibits two

relaxation peaks, one at a lower frequency below 1 kHz and another one at a higher frequency above 100 kHz. From the literature, it is noted down that in the investigated frequency range interfacial and dipolar, and polarizations contribute significantly to the dielectric constant/dissipation factor. Interfacial polarization in BTS sample may arise due to the presence of heterogeneities at micro level due to the random distribution of Sn at Ti site and due to the presence of grain and grain boundaries of different electronic nature. Since this sample was prepared at temperature 1350^{o}C, therefore there is the possibility of oxygen vacancies. Dipolar polarization in BTS sample arises due to the presence of dipoles like Sn^{4+} Sn^{2+} $''$ - $V_O^{\bullet\bullet}$ in the sample. The presence of higher frequency peak in D vs. log f plot of the composite may arise due to hopping of electrons between different valence states of nickel and iron present in the ferrite. Hopping conduction is a thermally activated process. As temperature increases, the hopping of electron between Fe^{3+} and Fe^{2+} ions is enhanced. On application of the external electric field, dipoles Fe^{2+} - Fe^{3+} orient their axes parallel to the applied field, thus contributing towards polarization.

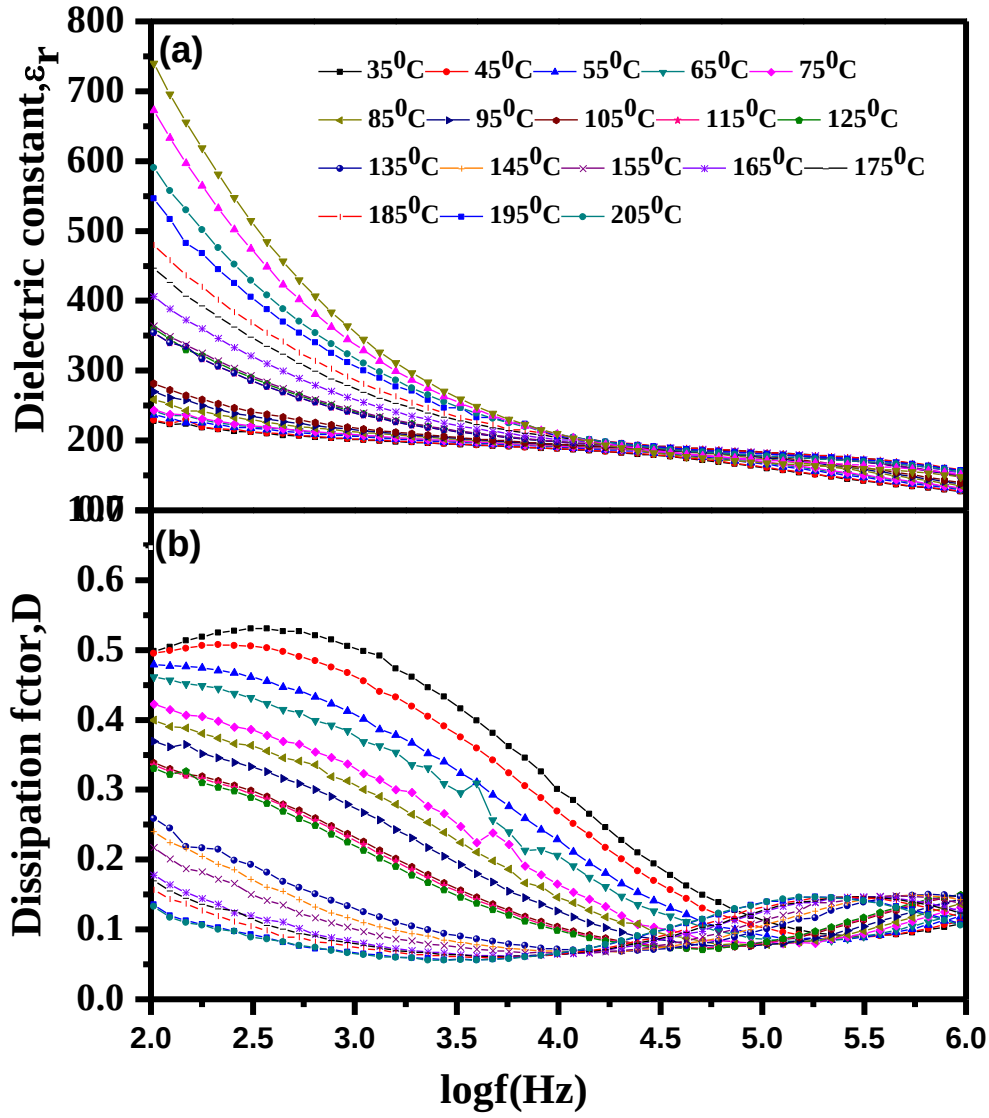

Figure 5.9 For BTS+NF15 variation of (a) Dielectric constant and (b) Dissipation factor with logarithm of frequency at different temperatures

Figure 5.10 [(a) , (b)] show room temperature ferroelectric hysteresis loops for the relaxor phase $BaTi_{0.85}Sn_{0.15}O_3$ (BTS) and one of the composites BTS+NF15 at the differently poled field. It can be seen from the figure that both the samples exhibit typical ferroelectric hysteresis which indicates that the samples are spontaneously polarized. The ferroelectric behavior of the

composite is weaker than for the BTS. The ferroelectric coercive field (EC) of the composite decreases with an increase of NF content, which implies that the composites are being easily polarized under the applied electric field. The observed PE hysteresis loops of BTS had no saturation and explained lossy capacitors behavior which is in confirmation with results obtained from conductivity and dissipation factor measurements and discussed above.

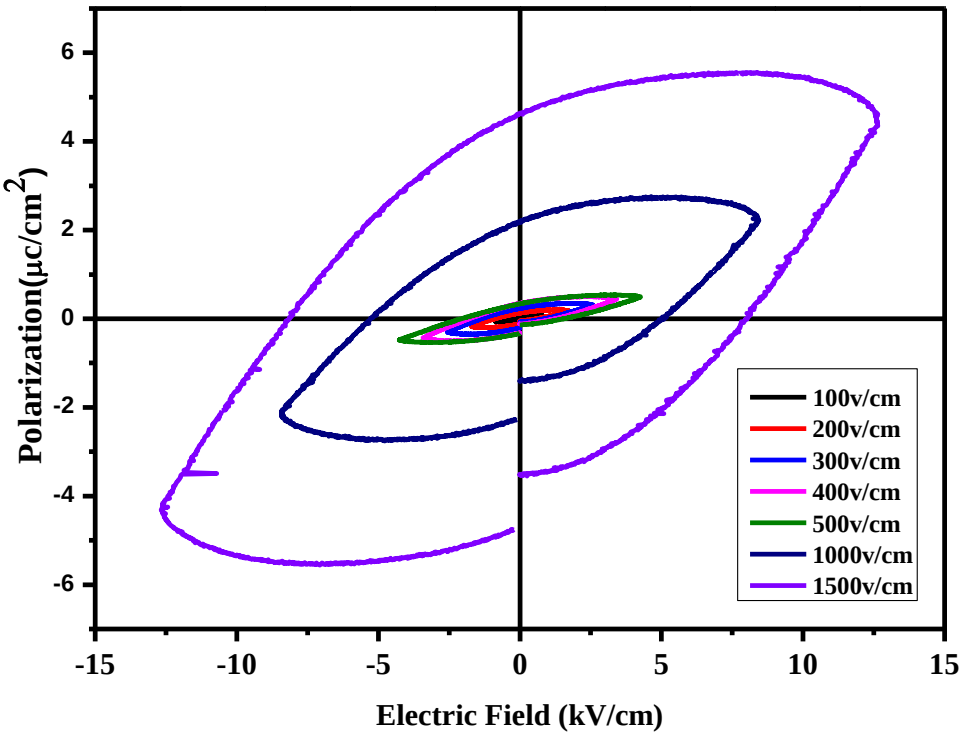

Figure 5.10 (a) Room temperature P-E loop of $BaTi_{0.85}Sn_{0.15}O_3$

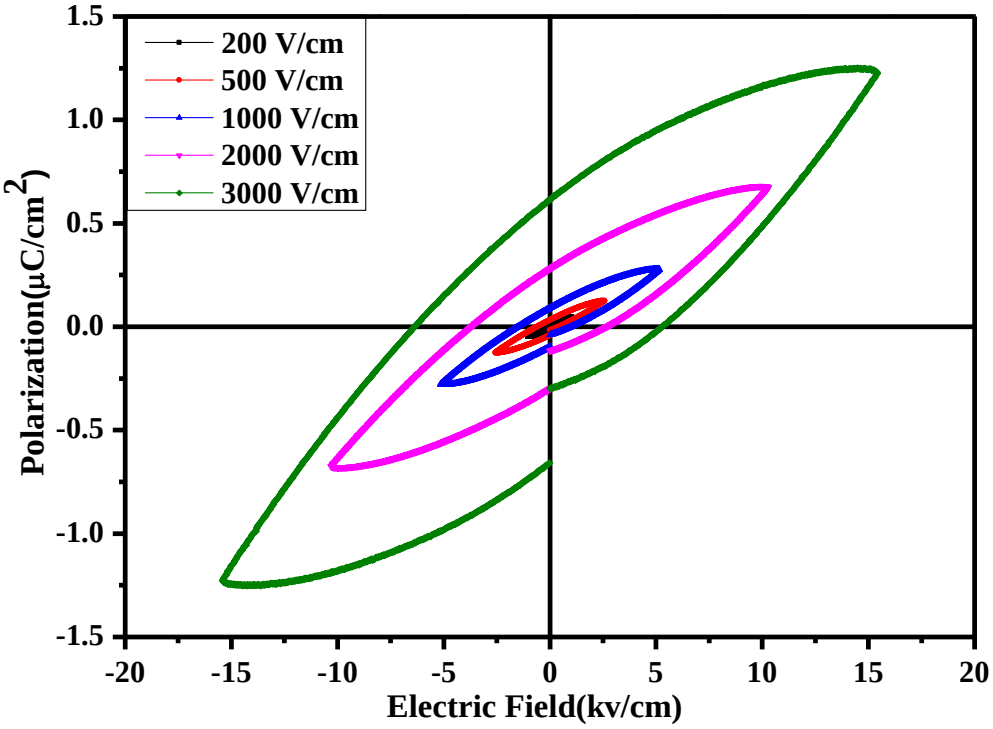

Figure 5.10 (b) Room temperature P-E loop of the composite BTS+NF15

5.2.9 Magnetic Properties

Room temperature magnetic field dependence of the magnetization (M-H curves) of NF and four composite samples have been recorded within the range of magnetic field ± 20 kOe and shown in Figure 5.11 (a) and (b). M-H curve of NF and composites showed thin hysteresis loop as it is observed from zoom view of M-H curve at the low magnetic field and shown in the inset of Figure 5.11(a) and (b). The composites also exhibit typical magnetic hysteresis similar to nickel ferrite (NF), indicating that the composites are also magnetically ordered materials.From the hysteresis loops shown in Figure 5.11 (a) and (b), the value of spontaneous magnetization (Ms) of the samples was obtained by extrapolating the high-field linear part of the magnetization curve to zero fields and reported in Table 5.3. The values of other magnetic parameters such as remnant magnetization (Mr) and coercive field (Hc) of ferrite (NF) and composites are obtained

from their loops are also shown in Table 5.3. The variation of the saturation magnetization (M_s) and coercive field (Hc) with a concentration of ferrite phase (NF) in the composite, x is plotted in the bottom inset of Figure 5.11 (b). It is observed that the saturation magnetization of the composites decreases almost linearly with increasing $BaTi_{0.85}Sn_{0.15}O_3$ (BTS) content, the phenomenon is consistent with that reported in the literature [185]. This indicates that BTS is nonmagnetic nature and stops continuity of $NiFe_2O_4$ (NF) ferrite and hence magnetic moment of the composites decreases with increase the $BaTi_{0.85}Sn_{0.15}O_3$ (BTS).

In the literature, it has been suggested that the room temperature ferromagnetism/ferrimagnetism in intrinsically n-type semiconductor and insulators involves a model wherein shallow donor electrons, created due to intrinsic defects in the semiconductors, a form bound magnetic polarons (BMPs) with magnetic cations [186]. According to the BMPs model, the magnetization is given by:

$$M = M_0 L(x) + \chi_m H \qquad (5.4)$$

Where the first term is the contribution of magnetization due to the presence of BMPs and a second term due to paramagnetic interaction.Here $M_0 = N m_s$, N is the number of BMPs involve in magnetism and m_s is the effective spontaneous magnetic moment per BMP. $L(x)$is Langevin function given by:

$$L(x) = Coth(x) - 1/x \qquad (5.5)$$

Where$x = m_{eff} H/k_B T$ where m_{eff} is the true spontaneous magnetic moment per BMP, and at high temperature it can be approximated to $m_s = m_{eff}$. M-H curves shown in Figure 5.11 (a) and (b) have been fitted using Equation (5.5) by considering parameters $M_0, \chi_m, and\ m_{eff}$ as variables during fitting. The best fitting results are shown as solid lines in Figure 5.11 (a) and (b). Parameters obtained from the fitting are listed in Table 5.3. From the Table 5.3 it is noted

down that the value of saturation magnetization (M_s) of the synthesized nickel ferrite (NF) is 49.9 emu/g, slightly lower than 55 emu/g reported for the multi-domain bulk $NiFe_2O_4$ [187]. NF sample exhibits nearly zero remnantmagnetization (0.2 emu/g) andzero coercive field (1.1 Oe) suggesting a super-paramagnetic behavior. From the literature survey it is noted down that though, Ms and H_C are intrinsic properties of magnetic materials, but different preparation methods and conditions affects their values for $NiFe_2O_4$ [188]. Slightly lower value of saturation magnetization (compared to that for the multidomain bulk $NiFe_2O_4$) can be justified by the presence of some of the particles of nano-size in the synthesized $NiFe_2O_4$ powder as it is obvious from the SEM (Figure 5.4). It may be understood on the basis of core–shell model which predicts that in case of nanoparticles, the spins on the surface are canted (spin-glass-like surface layer) and hence the magnetization is reduced [189]. The spin glass shell leads to decrease of the number of aligned magneticmoment in the entire particles. The lower value of H_c observed for $NiFe_2O_4$ synthesized in this work may be due to the low shape anisotropy. Magnetic parameters of the composites are also presented in Table 5.3 which indicates that susceptibility of nickel ferrite and composite is of the order of 10^{-4} emu/g oe and sign is positive. The coercive field (H_c) and remnant magnetization (M_r) for all the composite samples is larger whereas saturation magnetization (M_s) is smaller than that for the pure $NiFe_2O_4$ as the results of mixing of non-magnetic phase BTS.

The theoretical values of Ms for the composites can be estimated using mixture, i.e., sum rule;

$$Ms(composites) = (1 - x)Ms(ferrite) + (x)Ms(ferroelectric) \quad (5.6)$$

Where *x* is the mole content of ferroelectric phase. Since for ferroelectric phase, Ms (ferroelectric) = 0

$$Ms(composites) = (1 - x)Ms(ferrite) \quad (5.7)$$

Experimental values of M_S for the composites are slightly less than the value calculated using mixture rule. This indicates that synthesized BTS is nonmagnetic (diamagnetic) in nature and spin present in the surface layers of ferrites particles in the composites have become more disordered. The disorder spin state increases magneto-crystalline energy which leads to increase in the coercive field (H_c) and remnant magnetization (M_r) and decreases the saturation magnetization Ms in the composites may be due to the enhancement in the surface spin disorder.

In order to test the existence of high field irreversibility, that is, the surface spin disorder, zero - field cooled (ZFC) and field cooled (FC) magnetization versus temperature curves were measured for synthesized NF and composite BTS+NF15 in H = 500 Oe from 2 to 300 K and shown in Figure 5.12 (a) and (b), respectively. For the ZFC measurements, the samples were cooled from room temperature to 2 K in zero magnetic fields, and the magnetization was recorded while warming the samples in the applied field. For the FC curves, the samples were cooled in the applied field from room temperature to 2K, and the magnetization was recorded in the same field with increasing temperature.As seen in Figure 5.12 (a) for NF, at low temperatures the magnetization in the FC curve is higher than that in the ZFC curve, and the two curves overlap when the temperature rises above the so-called irreversible temperature (T_{irr}).The irreversible temperature (T_{irr}) between ZFC and FC processes is found to be around 253 K for NF which is approximately equal to the literature value 255 K [148]. For the composite BTS+NF15, the T_{irr}temperature shifts above 300 K, and the difference between ZFC and FC curves has increased as compared to NF. The increase in T_{irr} may be due to the presence of diamagnetic BTS(similar to parent perovskite $BaTiO_3$) in the composite, being diamagnetic in nature, leads to a decrease in the effective magnetic field observed by NF. The increase in the separation between FC and ZFC curves below T_{irr} for the composite BTS+NF15 is due to

increase in the percentage of disorders of the spin present on the surface layer of ferrite. As already mentioned above, the spins on the surface can be found in a disordered state in ferrite nanoparticles. This fact can change the energy barrier that the particle must overcome to reach the magnetic saturation.

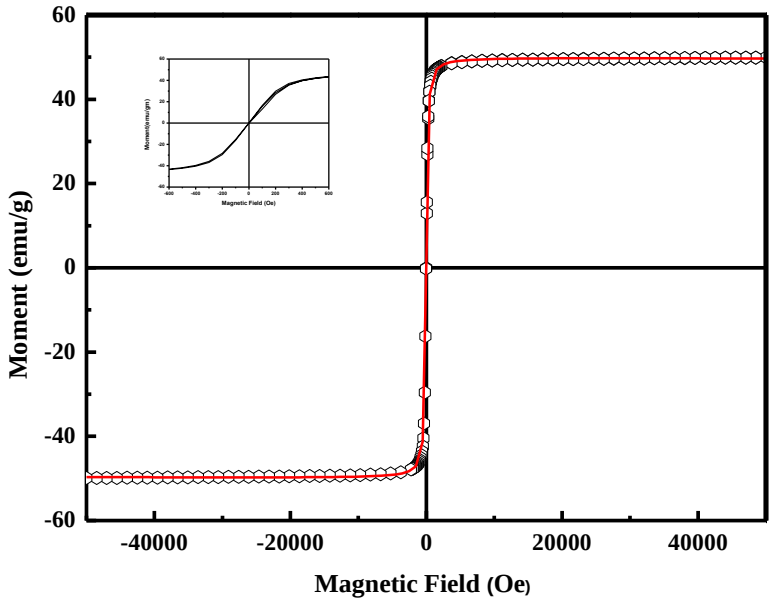

Figure 5.11(a) Room temperature M-H curve of $NiFe_2O_4$. The solid line is the fit curve

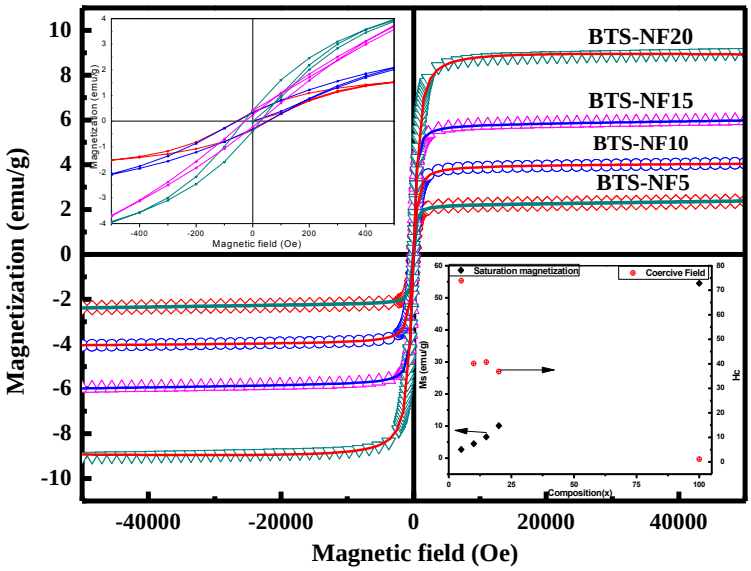

Figure 5.11(b) Room temperature M-H curve of composites. The solid lines are the fit curves

Table 5.3 Dielectric and Magnetic parameters of the constituent phases and their composites

Sample code	**Electrical parameters at room temperature**			**Experimental Result**			**Parameters obtained from BMP fitting**		
	ε_r at 1 kHz	**D at 1 kHz**	**log σ (S-cm^{-1}) At 20 Hz**	**Ms (emu/g)**	**H_c (Oe)**	**M_r**	**M_o (emu)**	**χ x 10^{-4} (emu/g Oe)**	**m_{eff}x 10^{-23} /cm^3**
NF	105	0.13	-8.1	1.09	0.27	8.97	49.15	17.4	5.48
BTS+NF5	655	0.11	-7.6	43.90	0.43	9.13	2.21	3.06	2.43
BTS+NF10	1176	0.16	-6.7	40.12	0.57	2.44	4.80	2.60	2.38
BTS+NF15	1851	0.08	-7.3	40.71	0.61	2.54	6.48	1.57	2.16
BTS+NF20	2022	0.13	-6.9	38.83	0.55	7.95	8.98	1.81	1.13
BTS	2684	0.17	-5.4			-		-	

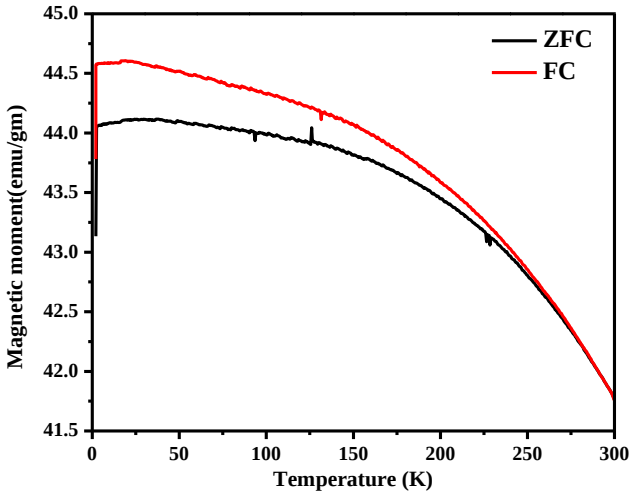

Figure 5.12 (a) ZFC and FC magnetization curves for end member $NiFe_2O_4$ in an applied field of 500 Oe.

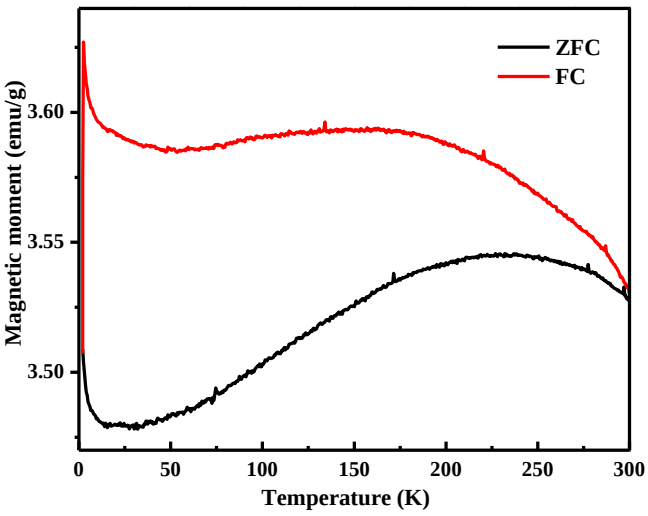

Figure 5.12 (b) ZFC and FC magnetization curves for the composite BTS+NF15 in an applied field of 500 Oe

5.3 CONCLUSIONS

Single phase powders of $BaTi_{0.85}Sn_{0.15}O_3$ and $NiFe_2O_4$ were synthesized successfully by solid state and Gel-combustion methods, respectively. Dense and homogeneous composites of $BaTi_{0.85}Sn_{0.15}O_3$ and $NiFe_2O_4$ were synthesized by solid state method. The formation of the composites and their constituents was confirmed by X-ray diffraction, FTIR and SEM analyses.Conduction in the samples is governed by hopping of electrons among the different ions of the elements Sn, Ti, Ni and Fe present in the BTS and composites. Variation of dielectric constant with respect to frequency shows a dispersive behavior due to Maxwell-Wagner effect. The interfacial polarization has a significant contribution for composites as compared to BTS. A relaxation phenomenon in the high-frequency range was observed in the composites which are intrinsic properties of the composites. AC conductivity, dielectric constant and dissipation factor of the composites are smaller than that of BTS. BTS and composite BTS+NF15 exhibits ferroelectric hysteresis loop at room temperature. For the composite flattened P-E loops with smaller values of the saturation polarization and larger value of coercive electric field were obtained as compared to BTS. Synthesized Nickel ferrite is in superparamagnetic state at room temperature. Composites are also magnetically ordered system. The value of saturation magnetization increases linearly with increasing concentration of ferrite phase in the composite. However, the coercive field (Hc) and remnant magnetization (M_r) for all the composite samples is larger than that of pure $NiFe_2O_4$ phase.The value of saturation magnetization and coercive field indicates that composites are soft magnetic materials. The composite may be used in transformer, inductor cores, recording heads, microwave devices and magnetic shielding.